Letter

Longitudinal electromagnetic waves with extremely short wavelength

Denis Sakhno, Eugene Koreshin, and Pavel A. Belov*
Department of Physics and Engineering, ITMO University, Kronverksky prospekt 49, 197101 Saint Petersburg, Russia

(Received 19 March 2021; revised 29 July 2021; accepted 7 September 2021; published 20 September 2021)

Electromagnetic waves in vacuum and most materials have transverse polarization. Longitudinal electromagnetic waves with an electric field parallel to the wave vector are very rare and appear under special conditions in a limited class of media, for example, in plasmas. In this Letter, we study the dispersion properties of an easy-to-manufacture metamaterial consisting of two three-dimensional cubic lattices of connected metallic wires inserted one into another, also known as an interlaced wire medium. It is shown that the metamaterial supports longitudinal waves at an extremely wide frequency band from very low frequencies up to the Bragg resonances of the structure. The waves feature unprecedentedly short wavelengths comparable to the period of the material. The revealed effects highlight a spatially dispersive response of the interlaced wire medium and provide a route toward generating electromagnetic fields with strong spatial variations.

DOI: 10.1103/PhysRevB.104.L100304

Elastic waves may have either longitudinal or transverse polarization: The acoustic (compression) waves are longitudinal while the sheer stress waves are usually transverse. The electromagnetic waves are in many aspects similar to the elastic ones. However, most of the electromagnetic waves are transverse. The longitudinal wave has a wave vector $\mathbf{k}$ parallel to the electric field $\mathbf{E}$. Substitution of such conditions into Maxwell's equations for nonmagnetic isotropic media immediately leads to $\mathbf{H} = \mathbf{0}$ and $\varepsilon = 0$. This means that longitudinal electromagnetic waves may exist in homogeneous media only if the dielectric permittivity is equal to zero. Such a case can be reached in plasmas or plasmalike media also known as epsilon-near-zero (ENZ) materials [1–3].

The longitudinal wave in such a case is called a bulk plasmon [4], and it exists at a particular frequency ω_p called a plasma frequency defined by the equation $\varepsilon(\omega_p) = 0$. Due to frequency dispersion, the condition $\varepsilon(\omega) = 0$ can be satisfied only at fixed frequencies. However, spatial dispersion effects (nonlocality), manifested as the dependence of permittivity on the wave vector of a propagating wave $\varepsilon(\omega, \mathbf{k})$, allows bulk plasmons to exist within a certain very narrow frequency band [4,5].

In natural media the effects of spatial dispersion are extremely weak since the period of the crystal is significantly smaller than the wavelength. The bandwidth of the bulk plasmon band is only a few percent of the respective frequency [4,5]. Metamaterials which are artificially synthesized media [6] feature typically stronger spatial dispersion effects since their periods are comparable to 10^{-1}–$10^{-2}\lambda$. For instance, a connected wire medium, also known as an artificial plasma [7], supports bulk plasmons within a 7% band near the plasma frequency [8–10].

Spatial dispersion effects are boosted when the ratio between the period of the structure and wavelength increases. For example, the effect of spatial-dispersion-induced birefringence quantified by the difference of the refractive indices for two orthogonal polarizations in a metamaterial with cubic symmetry can reach 0.13 in resonant metamaterials as compared to 10^{-5} in natural crystals such as CuI or NaI [11]. However, the discussed spatial dispersion effects are observed within a quite narrow frequency range close to the characteristic resonances of a metamaterial.

The exception from this general rule is provided by the nonconnected wire media [12], which are metamaterials formed by parallel arrays of infinitely long wires disconnected from each other. Nonconnected wire media feature a very strong spatial dispersion within an extremely wide frequency range including the long-wavelength limit [13]. Their nonlocal electromagnetic response results in diffractionless transverse electromagnetic waves with arbitrary transverse wave vectors which can be used for subwavelength imaging [14] and improvement of magnetic resonance imaging systems [15].

In this Letter, we investigate the properties of a special class of wire media, the so-called interlaced wire media [16–18]. The geometry of the medium is shown in Fig. 1(a): It consists of two three-dimensional (3D) wire meshes embedded one into another without an electrical connection between the meshes. Due to this, the interlaced wire medium at low frequencies in many ways differs from a single 3D wire metamaterial [7–10]. Basically, 3D wire metamaterials feature inductive behavior whereas an interlaced wire medium following Ref. [16] behaves more as a transmission line with both inductive and capacitive behavior, where the effective capacitance is associated with the two nonconnected submeshes.

Below, we demonstrate that such a structure supports longitudinal waves within an extremely wide frequency band starting from very low frequencies up to at least a frequency corresponding to a wavelength which is six times greater than the period of the metamaterial. Due to the pronounced spatially dispersive response of the interlaced wire medium, the

*belov@metalab.ifmo.ru

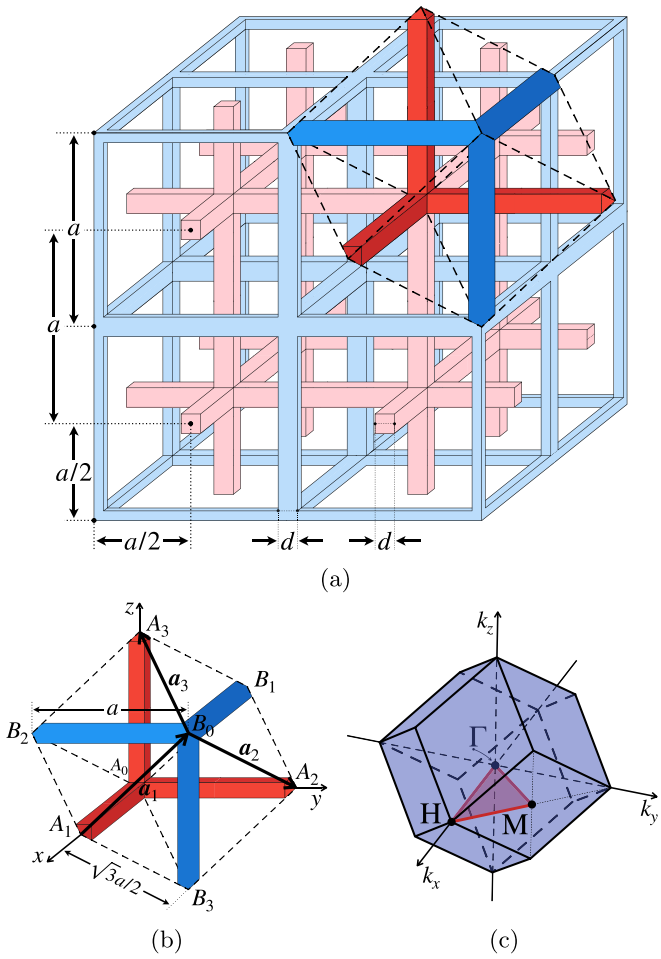

FIG. 1. (a) Geometry of the interlaced wire medium. (b) Rhombohedral unit cell of the metamaterial. Translation vectors coordinates: $A_1B_0 = (-a/2, a/2, a/2)^{\mathrm{T}}$, $B_0A_2 = (-a/2, a/2, -a/2)^{\mathrm{T}}$, $B_0A_3 = (-a/2, -a/2, a/2)^{\mathrm{T}}$. (c) Brillouin zone corresponding to the unit cell. Point coordinates: $\Gamma = (0, 0, 0)^{\mathrm{T}}$, $H = (2\pi/a, 0, 0)^{\mathrm{T}}$, $M = (\pi/a, \pi/a, 0)^{\mathrm{T}}$.

equation $\varepsilon(\omega, \mathbf{k}) = 0$ has solutions nearly at all frequencies below the first Bragg resonance. Interestingly, the wave vectors of the waves are very large, pointing to the corners of the first Brillouin zone of the metamaterial. It should be stressed that such behavior is quite unusual for electromagnetic waves since in the majority of materials low frequencies are related to short wave vectors of the wave such that isofrequency contours are centered around the $\Gamma = (0, 0, 0)^{\mathrm{T}}$ point of the Brillouin zone.

We consider a metamaterial consisting of two identical, perfectly conducting cubic wire meshes with a period a and $d \times d$ square cross section ($d = 0.1a$) inserted one into the other [Fig. 1(a)] and fixed in a position with a maximal distance between the network nodes [the network displacement vector $A_0B_0 = 0.5a(1, 1, 1)^{\mathrm{T}}$—see Figs. 1(a) and 1(b)]. The entire structure is placed in an isotropic host medium (vacuum). We consider here two identical connected wire meshes, contrary to the previous work [17] where wires in the meshes had different radii.

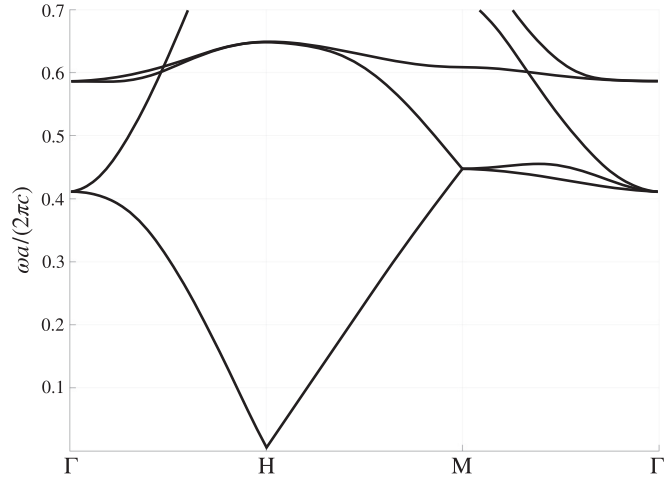

FIG. 2. Dispersion diagram for the $\Gamma HM\Gamma$ path. Brillouin zone point coordinates: $\Gamma = (0, 0, 0)^{\mathrm{T}}$, $H = (2\pi/a, 0, 0)^{\mathrm{T}}$, $M = (\pi/a, \pi/a, 0)^{\mathrm{T}}$.

The structure has body-centered-cubic (bcc) symmetry [in nature some metals such as lithium (Li), chromium (Cr), tungsten (W), and some others have such a crystal structure, canonical bcc] and belongs to the O_h symmetry group. Figure 1(b) shows the geometry of the unit cell for the interlaced wire metamaterial and how it is related to the structure of the medium [Fig. 1(a)]. This unit cell is rhombohedral, i.e., a hexagon with equal rhombuses at all faces, where all ribs are equal to $\sqrt{3}a/2$. One of two diagonals at each face contains a metal wire of length a. This rhombohedral cell is well known in solid state physics as a *primitive* cell for bcc crystal structures. The coordinates of the vertices can be written as

$$\begin{aligned} A_0 &= (0, 0, 0)^{\mathrm{T}}, \quad & B_0 &= (a/2, a/2, a/2)^{\mathrm{T}}, \\ A_1 &= (a, 0, 0)^{\mathrm{T}}, \quad & B_1 &= (-a/2, a/2, a/2)^{\mathrm{T}}, \\ A_2 &= (0, a, 0)^{\mathrm{T}}, \quad & B_2 &= (a/2, -a/2, a/2)^{\mathrm{T}}, \\ A_3 &= (0, 0, a)^{\mathrm{T}}, \quad & B_3 &= (a/2, a/2, -a/2)^{\mathrm{T}}. \end{aligned} \tag{1}$$

The translation vectors are

$$\boldsymbol{a}_1 = A_1B_0, \quad \boldsymbol{a}_2 = B_0A_2, \quad \boldsymbol{a}_3 = B_0A_3. \tag{2}$$

The interlaced wire medium with the described unit cell has a complex 12-sided Brillouin zone (rhombic dodecahedron) shown in Fig. 1(c).

We have calculated dispersion properties for the interlaced wire medium using the commercial software package COMSOL MULTIPHYSICS by applying periodic boundary conditions (with $e^{+i(\mathbf{k}\cdot\mathbf{r})}$ spatial dependence) to the unit cell with the wave vector $\mathbf{k}$ spanning the first Brillouin zone. As a result, we have calculated the respective eigenfrequencies $\omega(\mathbf{k})$. The dispersion properties of the studied metamaterial are illustrated by (1) the dispersion diagram shown in Fig. 2, (2) the isofrequency contours in the k_xk_y plane for a set of five frequencies shown in Fig. 3, and (3) the isofrequency surfaces for a single frequency shown in Fig. 4.

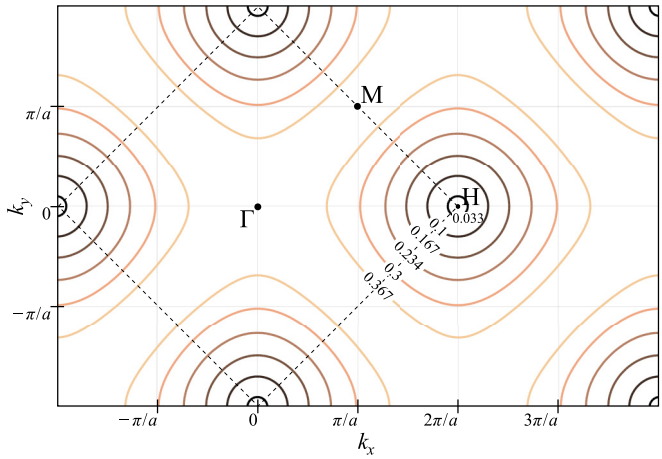

FIG. 3. Isofrequency contours in the k_xk_y plane. The frequencies on the contours are pointed in normalized units of $2\pi c/a$.

According to these results, it is discovered that at low frequencies the isofrequency surfaces of the metamaterial surround the corners (H points) of the Brillouin zone, but not the Γ point as in Refs. [16–18]. This means that the metamaterial supports waves with extremely large wave vectors at low frequencies. As one can see from the dispersion diagram in Fig. 2, the metamaterial has an artificial plasma frequency [8–10] around $\omega = 0.41 \cdot 2\pi c/a$. However, contrary to the case of a three-dimensional connected wire medium, the bulk plasmon mode branch (which usually exists below the plasma frequency) bends down to zero at the H point. Despite the unexpectedness of such results due to the seemingly isotropic nature of the material, this conclusion can be justified theoretically.

To this end, following the approach of Ref. [19], we consider the low-frequency limit when the wave equation is converted to the Poisson's equation, when the latter can be written in terms of electrostatic potentials. Since two wire sublattices are not connected, they should have distinct potentials φ_1 and φ_2.

On the other hand, the periodic nature of the system requires that the potential difference between the two sublattices

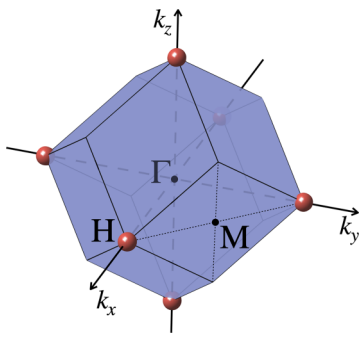

FIG. 4. Isofrequency surfaces at the first Brillouin zone for $\omega = 0.05 \cdot 2\pi c/a$ (red spheres).

should satisfy Bloch's theorem, which yields

$$\begin{aligned}(\varphi_1 - \varphi_2) &= (\varphi_2 - \varphi_1)e^{i(\mathbf{k}\cdot\boldsymbol{a}_1)},\\ (\varphi_1 - \varphi_2) &= (\varphi_2 - \varphi_1)e^{i(\mathbf{k}\cdot\boldsymbol{a}_2)},\\ (\varphi_1 - \varphi_2) &= (\varphi_2 - \varphi_1)e^{i(\mathbf{k}\cdot\boldsymbol{a}_3)}.\end{aligned} \tag{3}$$

Each of the equations in (3) relates the potential difference between meshes at the opposite surfaces of the rhombohedral cell. For example, Fig. 1(b) suggests that $A_0B_2A_1B_3$ coincides with $B_1A_3B_0A_2$ when shifted by a vector $\boldsymbol{a}_1$. Similarly, Bloch's theorem can be applied for the other two pairs of opposite faces.

The system of equations (3) is equivalent to the following conditions,

$$T \cdot \mathbf{k} = \begin{pmatrix}2n_1+1\\2n_2+1\\2n_3+1\end{pmatrix}\pi, \quad n_1, n_2, n_3 \in \mathbb{Z}, \tag{4}$$

where

$$T = \begin{pmatrix}\boldsymbol{a}_1^{\mathrm{T}}\\\boldsymbol{a}_2^{\mathrm{T}}\\\boldsymbol{a}_3^{\mathrm{T}}\end{pmatrix} = a/2\begin{pmatrix}-1 & 1 & 1\\-1 & 1 & -1\\-1 & -1 & 1\end{pmatrix}. \tag{5}$$

Hence, it is straightforward to show that

$$\begin{pmatrix}k_x\\k_y\\k_z\end{pmatrix} = \begin{pmatrix}n_2+n_3+1\\n_3-n_1\\n_2-n_1\end{pmatrix}\frac{2\pi}{a}, \quad n_1, n_2, n_3 \in \mathbb{Z}. \tag{6}$$

Depicting the set of solutions corresponding to Eq. (6) in reciprocal space, we observe that the isofrequency surfaces emerge from the H points as in Fig. 4. Importantly, no isofrequency surfaces appear at the point Γ since $k_x = k_y = k_z = 0$ is not the solution of Eq. (6).

Thus, we have proved both numerically and analytically that the interlaced wire medium supports the modes with a large wave vector at low frequencies. In order to determine the polarization state of of these modes, we have calculated the average electric field numerically by taking into account the phase shift due to the wave vector [20],

$$\mathbf{E}^{\mathrm{av}} = \frac{1}{V_{\mathrm{unit\ cell}}}\int_{\mathrm{unit\ cell}} \mathbf{E}(\mathbf{r}) \cdot e^{-i\mathbf{k}\cdot\mathbf{r}} dV, \tag{7}$$

where $\mathbf{r}$ provides the coordinates of the point inside the unit cell, $\mathbf{E}(\mathbf{r})$ is the electric field at this point, and $\mathbf{k}$ is the wave vector for which the eigenmode is calculated.

The result of averaging of the electric field for the wave vectors corresponding to a single low-frequency isofrequency contour is illustrated in Fig. 5(a). One can clearly see that the mode is longitudinal, i.e., the vector $\mathbf{k}$ is parallel to the vector $\mathbf{E}^{\mathrm{av}}$. In order to accurately assess the polarization of the mode, we calculated the longitudinal coefficient

$$\chi_{\mathbf{k}\|\mathbf{E}^{\mathrm{av}}} = \frac{(\mathbf{k}\cdot\mathbf{E}^{\mathrm{av}})}{|\mathbf{k}||\mathbf{E}^{\mathrm{av}}|} \tag{8}$$

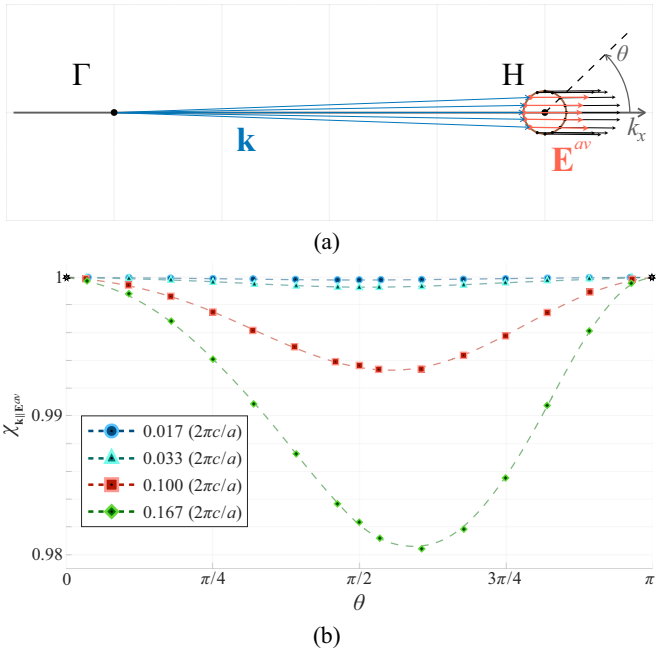

FIG. 5. (a) Isofrequency contour $\omega = 0.033 \cdot 2\pi c/a$ with the designation of Γ and H points on it and vectors of the average electric field $\mathbf{E}^{\text{av}}$ and $\mathbf{k}$. (b) Plot of the dependence of the longitudinal wave ratio $\chi_{\mathbf{k}\|\mathbf{E}^{\text{av}}}$ on the angular coordinate θ of a point on the contour (the angle between k_x and the vector drawn from the H point) for different frequencies.

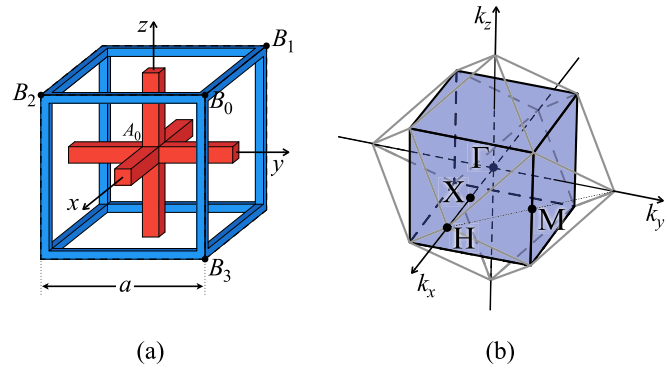

FIG. 6. (a) Cubic supercell of the metamaterial. (b) Cubic Brillouin zone corresponding to the supercell inside the rhombic dodecahedron Brillouin zone for the primitive unit cell. Point coordinates: $\Gamma = (0, 0, 0)^{\text{T}}$, $X = (\pi/a, 0, 0)^{\text{T}}$, $H = (2\pi/a, 0, 0)^{\text{T}}$, $M = (\pi/a, \pi/a, 0)^{\text{T}}$.

as a function of the angular coordinate θ of a point on the contour at a given frequency [see Fig. 5(b)]. By the definition, the closer the longitudinal coefficient is to one, the smaller is the angle between the electric field and the wave vector.

As one can see from Fig. 5(b), with the decrease of the frequency the curve of the longitudinal coefficient approaches 1. The maximum deviation from the longitudinal polarization is less than 2% for $\omega = 0.167 \cdot 2\pi c/a$ and less than 1% for $\omega = 0.1 \cdot 2\pi c/a$. Thus, the low-frequency modes of the interlaced wire medium are longitudinal.

In Refs. [16,18] the authors considered the same interlaced wire medium structure as in this Letter, but it was assumed that the unit cell of the structure has a cubic shape as in Fig. 6(a). The cubic supercell is two times larger in volume than the primitive unit cell [Fig. 1(b)]. This doubling of the primitive unit cell results in a double decrease of volume of the Brillouin zone [Fig. 1(c)] and a change from a rhombic dodecahedron shape to a cubic shape as demonstrated in Fig. 7(b). The dispersion diagram along the ΓX path for the double supercell can be obtained from the corresponding dispersion diagram (Fig. 2) for the primitive unit cell by the operation of mirror reflection (flipping) as shown in Figs. 7(a) and 7(b). The flipping of the dispersion diagram is described in Ref. [21] where doubling of the unit cell is studied in detail. Note that this dispersion diagram is the same as the ones presented in Fig. 1(b) of Ref. [16] and in Fig. 1(f) of Ref. [18], and the dispersion diagram contains a branch starting from the Γ point at low frequencies. The isofrequency contours for the double supercell can be obtained from the corresponding isofrequency contours (Fig. 3) for the primitive unit cell by the operation of origami folding (flipping) as shown in Figs. 7(c) and 7(d).

It is simpler (both numerically and analytically) to consider an interlaced wire medium as a material with a cubic unit cell as in Fig. 6(a) and Brillouin zone as in Fig. 6(b), but this approach does not allow us to describe the dispersion properties of the interlaced wire metamaterial completely. For example, the use of a double supercell does not allow us to distinguish such points in the reciprocal space as Γ and H. Due to the Bloch theorem these points are equivalent within a double supercell description, but they are actually separate points of the Brillouin zone corresponding to the primitive unit cell [Fig. 1(c)]. However, as it was shown above, the metamaterial supports modes with large wave vectors (close to the H point) but does not support modes with small wave vectors (close to the Γ point) as it may seem from the dispersion diagrams [Fig. 7(b)] and isofrequency contours [Fig. 7(d)] for a cubic supercell.

In order to illustrate the importance of using a primitive unit cell instead of a cubic supercell, we have analyzed the spatial spectrum of typical eigenmodes supported by the metamaterial at low frequencies. The amplitudes of the Bloch harmonics $\mathbf{E}_{m,n,l}$ of an eigenmode $\mathbf{E}(\mathbf{r})$ were numerically calculated,

$$\mathbf{E}_{m,n,l} = \frac{1}{V_{\text{supercell}}} \int_{\text{supercell}} \mathbf{E}(\mathbf{r}) \cdot e^{-i\mathbf{k}_{\mathbf{m,n,l}} \cdot \mathbf{r}} dV, \qquad (9)$$

where $\mathbf{k}_{m,n,l} = \mathbf{k} + 2\pi/a(m, n, l)^{\text{T}}$, $m, n, l \in \mathbb{Z}$.

The spatial spectrum $\mathbf{E}_{m,n,l}$ of an eigenmode with $\omega a/2\pi c = 0.1$ and $\mathbf{k} = (0, 0.296, 0)^{\text{T}}\pi/a$ is shown in Fig. 8 for $m = -3 \ldots 3$, $n = -3 \ldots 3$, $l = 0$. One can see that the eigenmode has large amplitudes $\mathbf{E}_{0,-1,0}$, $\mathbf{E}_{-1,0,0}$, $\mathbf{E}_{0,1,0}$, and $\mathbf{E}_{1,0,0}$ while $\mathbf{E}_{0,0,0}$ is negligibly small. This means that the mode of the metamaterial does not have a spatial harmonic with a wave vector close to the Γ point in its spatial spectrum. The spectrum is dominated by harmonics

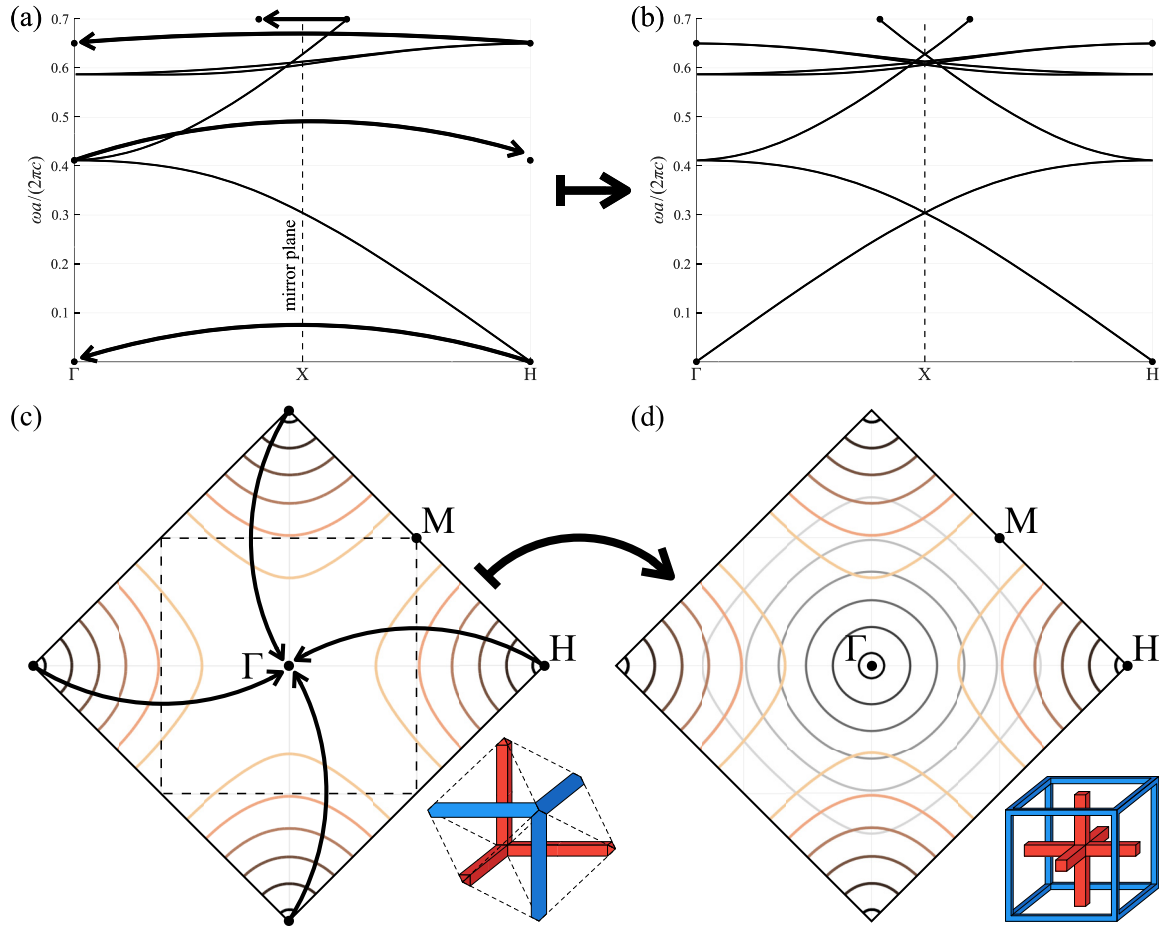

FIG. 7. (a) Dispersion diagram for the ΓXH path (same as in Fig. 2) for the primitive unit cell and the flipping scheme for obtaining (b) the dispersion diagram for the cubic supercell. (c) Isofrequency contours calculated for the primitive unit cell (same as in Fig. 3) and the flipping (origami folding) scheme for obtaining (d) the isofrequency contours for the cubic supercell. $\Gamma = (0, 0, 0)^{\mathrm{T}}$, $X = (\pi/a, 0, 0)^{\mathrm{T}}$, $H = (2\pi/a, 0, 0)^{\mathrm{T}}$, $M = (\pi/a, \pi/a, 0)^{\mathrm{T}}$.

with large wave vectors close to the points described by Eq. (6). Our numerical calculations demonstrate that such behavior of a spatial spectrum is typical for eigenmodes of an interlaced wire metamaterial at low frequencies and does not significantly depend on the direction of wave vector **k**.

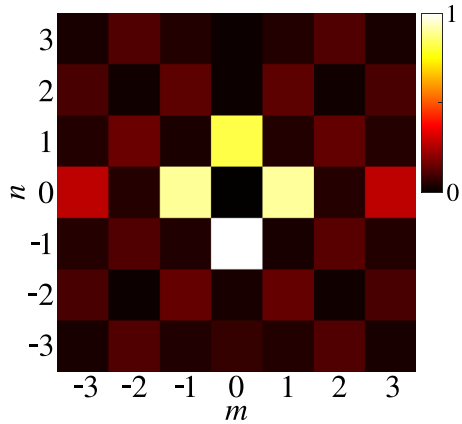

FIG. 8. Histogram of Bloch harmonics amplitudes $|\mathbf{E}_{m,n,0}|$ (normalized by maximum value) for an eigenmode corresponding to $\omega = 0.1 \cdot 2\pi c/a$ and $\mathbf{k} = (0, 0.296, 0)^{\mathrm{T}}\pi/a$.

In conclusion, in this Letter we have studied the dispersion properties of an interlaced wire medium in the symmetric configuration. As we have proved, this metamaterial supports low-frequency modes with large wave vectors and longitudinal polarization, which highlights the strongly nonlocal response of the structure. We believe that the control of the spatial dispersion effects in metamaterials will enable promising applications such as the recently demonstrated all-angle impedance matching [22,23], polarization control [18], imaging with subwavelength resolution [14], or squeezing the wavelength of electromagnetic fields, as suggested in this Letter, to enable forbidden transitions [24].

The authors are grateful to Maxim Gorlach for very fruitful discussions. This work was supported by the Russian Science Foundation. Theoretical models and numerical simulations were supported by the Grants No. 21-79-10209 and No. 20-72-10090, respectively.

[1] I. Liberal and N. Engheta, Nat. Photonics **11**, 149 (2017).
[2] X. Niu, X. Hu, S. Chu, and Q. Gong, Adv. Opt. Mater. **6**, 1701292 (2018).
[3] N. Kinsey, C. DeVault, A. Boltasseva, and V. M. Shalaev, Nat. Rev. Mater. **4**, 742 (2019).
[4] V. L. Ginzburg and J. B. Sykes, *The Propagation of Electromagnetic Waves in Plasmas* (Pergamon, Oxford, UK, 1964).
[5] G. Piazza, D. Kolb, K. Kempa, and F. Forstmann, Solid State Commun. **51**, 905 (1984).
[6] M. Kadic, G. W. Milton, M. van Hecke, and M. Wegener, Nat. Rev. Phys. **1**, 198 (2019).
[7] J. Brown, Proc. IEE **100**, 51 (1953).
[8] J. B. Pendry, A. J. Holden, D. J. Robbins, and W. J. Stewart, J. Phys.: Condens. Matter **10**, 4785 (1998).
[9] J. B. Pendry, A. J. Holden, W. J. Stewart, and I. Youngs, Phys. Rev. Lett. **76**, 4773 (1996).
[10] M. G. Silveirinha, Phys. Rev. B **79**, 035118 (2009).
[11] M. A. Gorlach, S. B. Glybovski, A. A. Hurshkainen, and P. A. Belov, Phys. Rev. B **93**, 201115(R) (2016).
[12] C. R. Simovski, P. A. Belov, A. V. Atrashchenko, and Y. S. Kivshar, Adv. Mater. **24**, 4229 (2012).
[13] P. A. Belov, R. Marques, S. I. Maslovski, I. S. Nefedov, M. Silveirinha, C. R. Simovski, and S. A. Tretyakov, Phys. Rev. B **67**, 113103 (2003).
[14] P. A. Belov, G. K. Palikaras, Y. Zhao, A. Rahman, C. R. Simovski, Y. Hao, and C. Parini, Appl. Phys. Lett. **97**, 191905 (2010).
[15] A. P. Slobozhanyuk, A. N. Poddubny, A. J. E. Raaijmakers, C. A. T. van den Berg, A. V. Kozachenko, I. A. Dubrovina, I. V. Melchakova, Y. S. Kivshar, and P. A. Belov, Adv. Mater. **28**, 1832 (2016).
[16] J. Shin, J.-T. Shen, and S. Fan, Phys. Rev. B **76**, 113101 (2007).
[17] H. Latioui and M. G. Silveirinha, Phys. Rev. B **96**, 195132 (2017).
[18] A. W. Powell, R. C. Mitchell-Thomas, S. Zhang, D. A. Cadman, A. P. Hibbins, and J. R. Sambles, ACS Photonics **8**, 841 (2021).
[19] W.-J. Chen, B. Hou, Z.-Q. Zhang, J. B. Pendry, and C.-T. Chan, Nat. Commun. **9**, 1 (2018).
[20] M. G. Silveirinha and C. A. Fernandes, IEEE Trans. Microwave Theory Tech. **53**, 1418 (2005).
[21] N. Kaina, F. Lemoult, M. Fink, and G. Lerosey, Nature (London) **525**, 77 (2015).
[22] K. Im, J.-H. Kang, and Q.-H. Park, Nat. Photonics **12**, 143 (2018).
[23] S. Horsley, Nat. Photonics **12**, 127 (2018).
[24] N. Rivera, I. Kaminer, B. Zhen, J. D. Joannopoulos, and M. Soljačić, Science **353**, 263 (2016).